Over 10% Efficient Wide Bandgap CIGSe Solar Cells on Transparent Substrate with Na Predeposition Treatment

Mohamed Ould Salem,* Robert Fonoll, Sergio Giraldo, Yudania Sanchez, Marcel Placidi, Victor Izquierdo-Roca, Claudia Malerba, Matteo Valentini, Diouldé Sylla, Angelica Thomere, Dah Ould Ahmedou, Edgardo Saucedo, Alejandro Pérez-Rodríguez, and Zacharie Jehl Li-Kao*

With the recent rise of new photovoltaic applications, it has become necessary to develop specific optoelectronic properties for thin-film technologies such as $Cu(In,Ga)Se_2$ and to take advantage of their high degree of tunability. The feasibility of efficient wide bandgap absorbers on transparent conductive oxide substrates is, in that context, of critical importance. Using an original approach based on a predeposition sodium treatment, $Cu(In,Ga)Se_2$ absorbers fabricated by sputtering and reactive annealing with a Ga to (Ga + In) content over 0.7 and an optical bandgap above 1.4 eV are deposited on transparent fluorine-doped tin oxide films, with the insertion of an ultrathin $MoSe_2$ layer preserving the contact's ohmicity. Different material characterizations are carried out, and a thorough Raman analysis of the absorber reveals that the sodium pretreatment significantly enhances the Ga incorporation into the chalcopyrite matrix, along with markedly improving the film's morphology and crystalline quality. This translates to a spectacular boost of the photovoltaic performance for the resulting solar cell as compared with a reference device without Na, specifically in the voltage and fill factor. Eventually, an efficiency exceeding 10% is obtained without antireflection coating, a record value bridging the gap with the state of the art on nontransparent substrates.

1. Introduction

$Cu(In,Ga)Se_2$ (CIGSe) solar cells have steadily improved in the past four decades, with a laboratory record efficiency of 23.35%[1] and a proven viability for large-scale industrial development.[2] Along with these impressive achievements, innovative photovoltaic applications and markets are being considered, among which building-integrated photovoltaics (BIPVs)[3] and the Internet of Things (IoTs)[4] are the most promising. Hence, the properties of existing standard solar cells will be, and already are in some respect, finely tuned to deliver the highest performance possible through this new paradigm. Characteristics such as mechanical flexibility, cell lightweightness, spectral absorption tunability, and transparency or bifacial properties are highly desirable features, for which thin-film technologies such as CIGSe have undeniable assets. The question of substrate transparency is critical in that regard, as it opens the door not only for both bifacial and semitransparent devices, but also to the realization of low-cost high-efficiency tandem solar cells.

M. Ould Salem, R. Fonoll, Dr. S. Giraldo, Dr. Y. Sanchez, Dr. M. Placidi, Dr. V. Izquierdo-Roca, Dr. D. Sylla, Dr. A. Thomere, Prof. E. Saucedo, Prof. A. Pérez-Rodríguez, Dr. Z. Jehl Li-Kao
Solar Energy Materials and Systems (SEMS)
Institut de Recerca en Energia de Catalunya (IREC)
1,2apl., Jardins de les Dones de Negre, 08930 Sant Adrià de Besòs
Barcelona, Spain
E-mail: msalem@irec.cat; zjehl@irec.cat

Dr. M. Placidi, Prof. E. Saucedo, Dr. Z. Jehl Li-Kao
Departament d'Enginyeria Electrònica
Universitat Politècnica de Catalunya
C/ Jordi Girona 1, 08034 Barcelona, Spain

Dr. C. Malerba, Dr. M. Valentini
ENEA
Casaccia Research Center
via Anguillarese 301, 00123 Roma, Italy

Prof. D. O. Ahmedou
Department of Physics
Faculty of Sciences and Techniques
University of Nouakchott Al Aasriya
5026 Nouakchott, Mauritania

Prof. A. Pérez-Rodríguez
Departament d'Enginyeria Electrònica i Biomèdica
IN2UB
Universitat de Barcelona
C/ Martí i Franqués 1, 08028 Barcelona, Spain

The fabrication of high efficiency CIGSe solar cells on transparent substrates is not new, and nearly two decades ago, the pioneering work from Nakada et al. in Japan[5] unequivocally demonstrated that the contact ohmicity could be preserved both on indium tin oxide (ITO) and fluorine-doped tin oxide (FTO) substrates by inserting an ultrathin Mo layer at the back interface. Recent reports of bifacial CIGSe solar cells on ZnO also exist albeit with comparatively lower efficiencies.[6]

Wide bandgap CIGSe solar cells, feasible by increasing the amount of Ga, are especially needed for potential applications as a top cell in low-cost tandem devices,[7] but high Ga-content devices have been long known to harbor more detrimental deep defects than their high In-content counterparts.[8,9] More importantly, the large majority of wide bandgap CIGSe absorbers currently reported are fabricated on opaque metallic Mo substrate, defeating the original purpose. Reported efficiencies are in the range of 11.0% for the pure $CuGaSe_2$ compound,[10] and range from 12% up to nearly 16% for CIGS compounds with 60–70% of gallium and bandgaps of 1.4–1.5 eV,[11–13] all these reports being on soda–lime glass (SLG)/Mo substrates. Very few wide bandgap devices have previously been made on transparent substrate, often with efficiencies well under their Mo-substrate counterparts.[14]

In this work, we propose to combine transparent FTO substrates and wide bandgap CIGSe absorbers ($E_g \geq 1.4\,eV$), and fabricate a proof of concept device with an efficiency exceeding 10% without antireflection coating. It is also worth noting that a deposition method based on metallic precursor sputtering and reactive thermal annealing was used, giving these results even more relevance for a fast technology transfer to the industry. Sodium doping is found to be a key parameter in the devices presented here, and in the course of this study, a comparison will be made with a reference sample, without Na. Moreover, the Na incorporation in the film follows an original approach, whereas postdeposition treatment (PDT) by an alkaline fluoride compound became the standard since the landmark publication from Tiwari and coworkers,[15] we instead propose here a predeposition treatment (PreDT), by evaporating 15 nm of NaF at the surface of the substrate before the fabrication of the CIGSe absorber. Glow discharge optical emission spectroscopy (GDOES) reveals a steep Ga grading with a single-slope profile, as opposed to the commonly reported double grading profile.[16] Using Raman spectroscopy, Na-doping is found as a driving parameter enhancing both the general crystalline quality of the films, but also the Ga incorporation in the matrix. From the scanning electron microscopy (SEM) images, a clearly

improved back contact is observed in the case of Na doping, and the fitting of the dark JV curves shows a general improvement in the diode parameters of the solar cells with Na PreDT. A record efficiency of 10.15% for a 1.41 eV bandgap is achieved on SLG/FTO substrate, with a Ga content in the absorber measured at 68% by X-ray fluorescence (XRF). This represents an absolute +1.6% increase in the efficiency ascribed to the Na PreDT. This result is, to the best of our knowledge, the highest reported efficiency for a wide bandgap CIGSe absorber grown on transparent substrate. To conclude this study, a short paragraph detailing improvement pathways will be presented.

2. Results and Discussions

2.1. Material Analysis

The SEM images of the sample #1 (with Na PreDT) and sample #2 (reference) with a similar magnification are shown in **Figure 1**. The morphology of both samples appears similar at first sight; both samples have a decrease in quality toward the back interface and a bilayer aspect is seen with much smaller grains. The back side of the absorber is where a Ga accumulation is expected;[17] those images hint at a possible phase segregation without the possibility to conclude on differences stemming from the presence of sodium. The complete set of SEM micrographs is presented at the end of the Supporting Information. To complement the visual observation, samples #1 and #2 are analyzed by X-ray diffraction, with a specific focus on the (112) and (220)/(204) peaks (**Figure 2**). A clear difference can now be made between both samples. Without Na, two different phases are observed, a feature particularly visible for the (112) peak (Figure 2b) with a Ga-poor and a Ga-rich contribution, indicating a strong inhomogeneity in the incorporation of Ga to the CIGSe matrix. In the presence of Na however, a well-defined single peak is shown in Figure 2b, a result consistent with a more homogeneous material and thus a better Ga incorporation to the CIGSe matrix. A phase segregation may still exist for this sample as the peak appears slightly asymmetric, but this possible segregation remains at a level low enough to be below the instrument's resolution. Regarding the (220)/(204) peaks shown in Figure 2c, a peak splitting is expected for high Ga content samples due to the c/a axis distortion of the tetragonal structure rather than phase separation;[18] in the case of sample #1 (with Na PreDT), two peaks are indeed observed, along with a much smaller shoulder at 45.55; the latter could be attributed to a limited phase
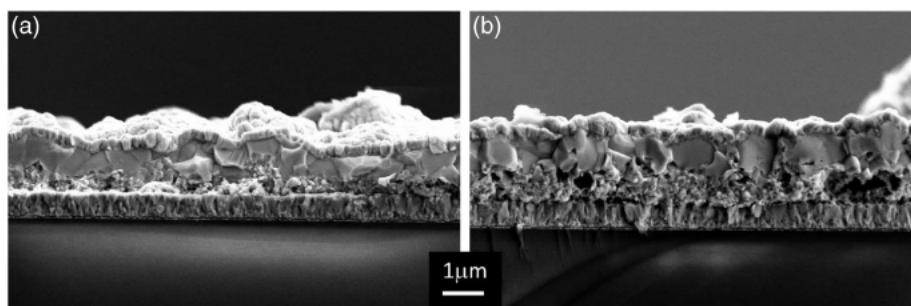
Figure 1. SEM images of the cross section in a) sample #1 and b) sample #2 with a 10k magnification.

2000284 (2 of 7)
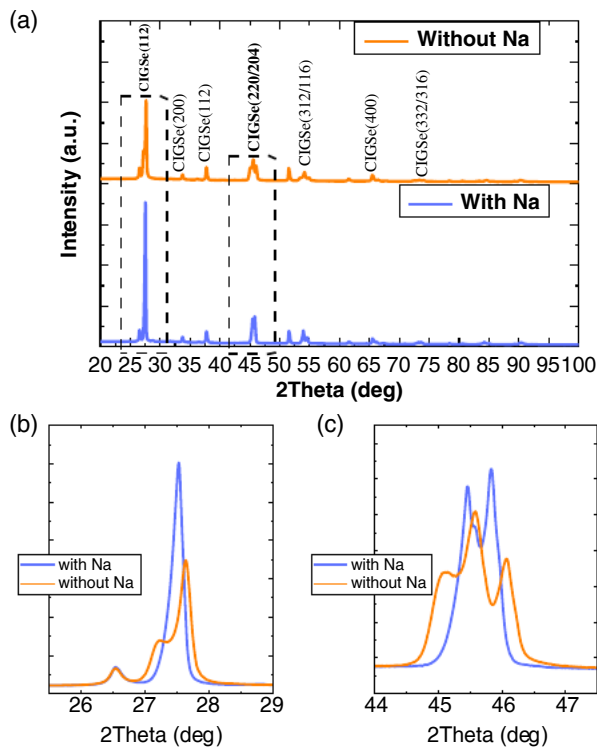
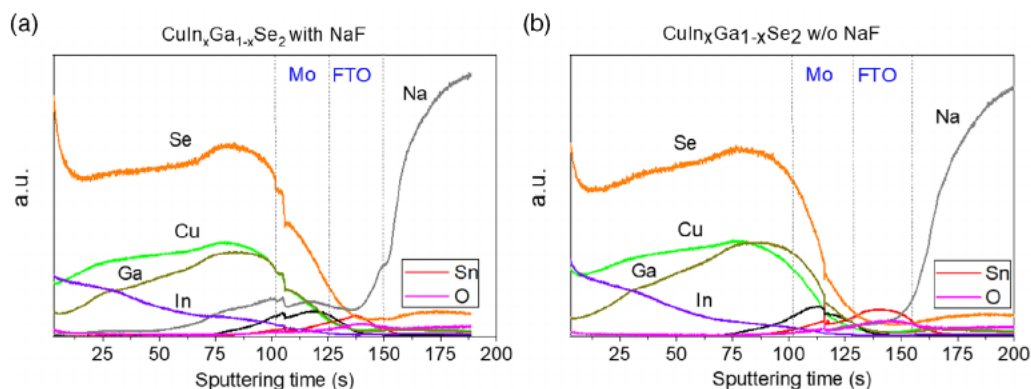**Figure 2.** XRD analysis of sample #1 and sample #2. a) Overview; b) 112 peak; and c) 220/240 peaks.

separation, which is not visible in Figure 2b. For sample #2, however (without Na), three well-defined peaks are visible, indicating again a clear phase separation between a Ga-poor and a Ga-rich layer, much more pronounced than in the presence of Na.

The samples' depth composition profile is investigated by GDOES analysis and shown in **Figure 3**a,b; several remarks can be made. For both samples #1 and #2, a Cu depletion is observed near the front interface, hinting at the presence of an ordered vacancy compound (OVC) phase though not unequivocally demonstrating it as GDOES lacks reliability close to the surface. Both samples exhibit a single Ga grading profile, with a steep accumulation toward the back interface, and without appreciable difference between both samples. Very little differences are observed in the In and Se profiles, a result anticipated as both

samples are processed within the same batch. The Na element is as expected present throughout the absorber for samples #1, whereas the analysis of sample #2 confirms that FTO is an efficient barrier for its diffusion from the SLG substrate. As a general observation, it is interesting to note that no sample shows specific features from an elemental depth composition viewpoint.

Raman spectroscopy is a valuable tool to dwell in the Na PreDT influence regarding the film properties, and we chose an approach based on two excitation wavelengths; a high energy excitation of 325 nm extremely sensitive to the samples' surface, and a more standard 532 nm excitation allowing a deeper probing of the films. The Raman spectra shown **Figure 4**a,b are for 325 and 532 nm excitation wavelengths, respectively, for sample #1 and sample #2. As explained in Experimental Section, a direct comparison between both excitations should not be made, and only a relative comparison between both samples at a given excitation wavelength is relevant. For both wavelengths, the spectra are characterized by a dominant peak around $180\,cm^{-1}$ followed by smaller contributions. The peak at $180\,cm^{-1}$ is identified with the A1 mode of the $Cu(In,Ga)Se_2$ in the chalcopyrite structure (space group $I\bar{4}2d$) with a [Ga]/([Ga]+[In]) ratio in the range of the 50–60%, consistent for both excitation wavelengths;[19,20] a value slightly lower than determined by XRF, but in line with the expectations, as it was shown that a significant part of the Ga is accumulated at the back side of the films. Additional weak contributions at 195, 223, 242, and $257\,cm^{-1}$ are observed for the 532 nm excitation (Figure 4b), and at $146\,cm^{-1}$ for the 325 nm excitation specifically (Figure 4a); identifying the origin of these contributions is not trivial. The $195\,cm^{-1}$ contribution can possibly be attributed to the Cu–Au $Cu(In,Ga)Se_2$ structure (space group $P\bar{4}M2$), showing similitudes with the very copper-poor $CuInS_2$ case.[21] This would however be, to our knowledge, the first time that such phase is reported in Ga-rich CIGSe samples, and caution should thus be exercised.

The $146\,cm^{-1}$ peak observed under UV conditions only (325 nm excitation, Figure 4a) has several possible interpretations. It can first be ascribed to a resonant enhancement effect of the $Cu(In,Ga)Se_2$; however, one should note that it could also be associated with the presence of an OVC rich in Ga.[22,23] To unequivocally identify the origin of this peak, a more detailed analysis using a known reference samples would be necessary. Finally, the complex structure in the region of the $200–260\,cm^{-1}$, which is visible for both excitations, is associated with the E and

Figure 3. Depth composition profiles of a) sample #1 and b) sample #2 determined by a glow discharge optical emission spectrometry analysis.
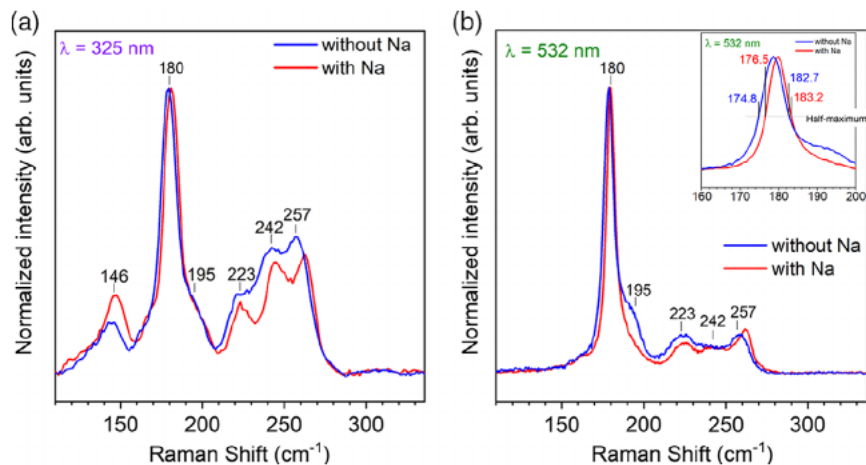
Figure 4. Raman spectra of sample #1 and sample #2 obtained using the a) 325 nm and the b) 532 nm excitation wavelengths.

B modes of the chalcopyrite structure of CIGSe and their variations are related to the ratio of the Ga/(Ga+In) in the CIGSe solid solution.[24] However, the overlapping of the OVC and Cu–Au contributions cannot be discarded.

The comparison of samples #1 and #2 spectra shows that clear differences exist between both. Focusing on Figure 4b (532 nm excitation) only, the main peak of the CIGSe is slightly shifted, suggesting a higher Ga ratio in the Na PreDT samples, possibly 5–10% higher. This agrees well with the shift and the relative intensity of the weak peaks in the 220–260 cm^{-1} region observed under 532 nm and the similar shift observed under 325 nm excitation. As the GDOES analysis showed a similar Ga elemental profile between both samples, this result tends to indicate a better Ga incorporation to the CIGSe matrix in the presence of Na close to the surface. This observation is consistent with previous work on Na doping of CIGSe absorbers.[25] Remarkably, the 195 cm^{-1} contribution associated with the Cu–Au structure is absent in sample #1 (Na PreDT sample) under 532 nm excitation, whereas it appears for both samples under 325 nm excitation. While the presence of this phase has been associated with a degradation of the devices' performance, previous studies by our group on CuInS$_2$ device[21] showed an improvement of the J_{sc}, but a reduction of the V_{oc}, and R_s. This was ascribed to a reduction of the defect concentration in the Cu-poor CuInS$_2$ by the accumulation of these defects in the more disordered Cu–Au phase, hence allowing a better crystalline quality in the chalcopyrite CuInS$_2$. It is unconfirmed if a similar conclusion is applicable here.
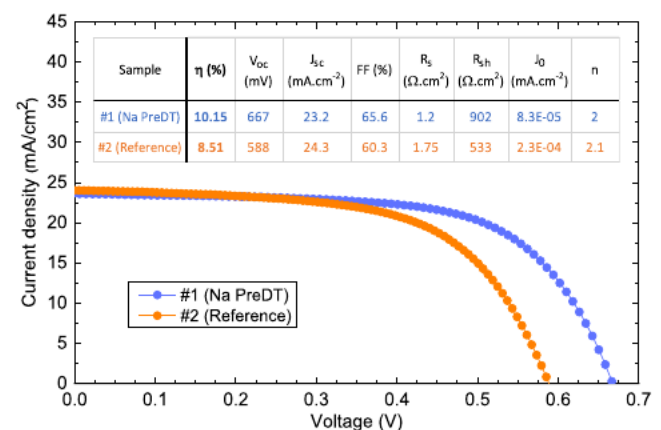
Focusing again on 532 nm excitation (Figure 4b), the full width at half maximum (FWHM) of the main 180 cm^{-1} peak is markedly reduced in sample #1 (from 7.9 to 6.7 cm^{-1}). This indicates that the Na PreDT is associated with an improvement of the crystal quality of the CIGSe, which would be in agreement with the reduction of the Raman contributions of the Cu–Au-disordered phase. Finally, a small shoulder in the 155–165 cm^{-1} region is observed in sample #1 (Figure 4b), and it is attributed to the presence of the OVC. This phase allows to accommodate the Cu-poor conditions of the absorber; the order of the defect in the structure allows to obtain an absorber with better optoelectronic properties.[26]

As a summary of the Raman analysis of the samples, two main observations should be kept in mind. The most important one is that Na PreDT significantly improves the Ga incorporation in the CIGSe structure (by 5–10% in our estimation), as shown by the peaks' shift for both excitation wavelengths; and second, a possible improvement of the general crystalline quality of the films can also be attributed to the Na doping, illustrated by the reduced FWHM of the 180 cm^{-1} peak in Figure 4b. A similar observation can, however, not be made in Figure 4a, and this should remain at this point an hypothesis as different interpretations (additional contributions) may exist for this FWHM difference.

2.2. Electrical Characterization of Devices

Solar cells are fabricated for samples #1 (with Na PreDT) and #2 (without Na) following the previously described standard process and electrically characterized by current–voltage analysis (JV) under AM1.5 illumination and dark conditions, and external quantum efficiency (EQE).

Figure 5 shows the JV characteristic of samples #1 and #2 along with their respective photovoltaic and diode parameters. A remarkable improvement of the performance is observed

Sample	η (%)	V_{oc} (mV)	J_{sc} (mA.cm^{-2})	FF (%)	R_s (Ω.cm^2)	R_{sh} (Ω.cm^2)	J_0 (mA.cm^{-2})	n
#1 (Na PreDT)	10.15	667	23.2	65.6	1.2	902	8.3E-05	2
#2 (Reference)	8.51	588	24.3	60.3	1.75	533	2.3E-04	2.1

Figure 5. Current voltage curves under illumination and diode parameters for sample #1 (Na PreDT) and sample #2 (reference).
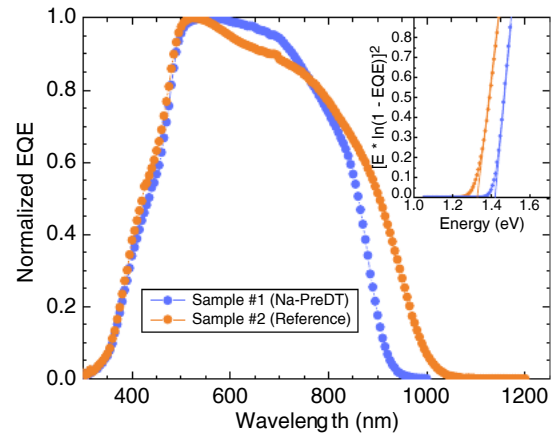
for the device with a Na PreDT; specifically, the fill factor jumps from 60.3% to 65.6%, and the V_{oc} is brought from 588 to 668 mV. A similar observation was made in the study by Wang et al.[22] regarding the influence of Na on these two parameters. While a slight reduction of the current is observed (from 24.3 mA cm^{-2} without PreDT down to 23.2 mA cm^{-2} for sample #1), the efficiency is markedly improved and reaches a record value of 10.15%. This value is the main result of this work, and it is to the best of our knowledge that the highest reported efficiency for a CIGSe solar cell on transparent substrate with a bandgap larger than 1.4 eV, getting close to those obtained with similar absorbers fabricated on metallic Mo substrates. It should also be noted that it was obtained without an antireflection coating, and there still exists a straighforward margin for improvement in that regard. **Table 1** shows an overview of the most relevant contributions in wide bandgap CIGSe solar cells; our device, albeit on transparent substrate, favorably compares with the highest reported values in terms of both efficiency and V_{oc}. The fitting of the dark JV curves using a single diode model reveals that both the shunt resistance and reverse saturation current are improved by the Na PreDT in sample #1. This observation is consistent with a possibly improved film morphology observed in the Raman analysis (Figure 4b). The Na PreDT, by improving the film's crystallinity, would reduce both the shunt pathways along with the density of recombination centers, the latter being closely related to J_0[30] yielding an overall superior diode performance.

The EQE analysis of samples #1 and #2 is shown in **Figure 6**, using EQE curves normalized to 1 for relative comparisons between both samples (see Experimental Section). A clear difference in the bandgap between both samples is visible, and while the GDOES composition analysis indicated a roughly similar GA profile in the films, such difference comes to no surprise; the X-ray diffraction (XRD) analysis indicated a clear phase separation in sample #2 (without Na), with a poor homogeneity in Ga incorporation and thus a Ga-poor phase reducing the bandgap of the absorber. Sample #1, in contrast, exhibited a more homogeneous Ga incorporation, resulting in a material with an overall higher bandgap. The Raman characterization additionally confirmed this observation that Na PreDT leads to a better Ga incorporation in the CIGSe. The normalized EQE onset at the vicinity of the bandgap is also steeper for sample #1, an indication of a better collection of charge carriers generated from low

Figure 6. Compared normalized external quantum efficiency of sample #1 and sample #2. Inset: bandgap determination plot $h\nu \times \ln(1-EQE)^2$ against $h\nu$.

energy photons, and thus of an improvement of the back interface's quality of the absorber. A result consistent with a material with a lower level of phase segregation is obtained.

For a direct bandgap, the absorption coefficient depends on $\alpha h\nu \propto (h\nu - E_g)^{\frac{1}{2}}$. Hence, a plot of $h\nu \times \ln(1-EQE)^2$ against $h\nu$ gives a reasonable extrapolation of the electronic bandgap E_g, as shown in the inset of Figure 6. Using Na PreDT, E_g is increased from 1.32 to 1.41 eV, an effect fully attributed to the more homogeneous Ga incorporation discussed during the XRD and Raman analysis, allowing the material to maintain a higher minimum bandgap.

The electrical characterization of our samples demonstrates that the Na PreDT permits the fabrication of wide bandgap CIGSe solar cells on a transparent substrate with performance rivaling the state of the art on metallic Mo substrate; it is, however, important to point out that some limitations and improvement pathways remain, which are discussed in the last part of this work.

2.3. Limitations and Improvement Pathways

The most critical improvement pathway lies in the actual transparency of the back contact. In this work, the MoSe$_2$ thickness was estimated to be 30–40 nm while still allowing for a certain level of transparency (45% at 700 nm in our case, see Figure S1, Supporting Information), our recent work on transition metal oxides reveals that the transparency of the back contact can potentially be doubled (Figure S2, Supporting Information), though electrical optimizations are still needed to improve the contact's ohmicity.

While beyond the scope of this work, other alkali elements are under evaluations for wide bandgap CIGSe films on FTO, with Rb and Cs being the most promising pathways for further improving the solar cell's performances. Wider bandgaps are also aimed at, with the hope that heavier alkali elements will allow for an even better Ga incorporation in the films. Similarly, a comparison between predeposition and the more standard postdeposition of the alkali element would bring valuable

Table 1. Summary of the photovoltaic properties of wide bandgap CIGSe solar cells as reported in relevant references, and compared with the record device from this work.

Ref	GIG [%] or E_g [eV]	Substrate	V_{oc} [mV]	J_{sc} [mA cm^{-2}]	FF [%]	E_{ff} (no ARC) [%]
[27]	67%	Mo	750	21	70	11
[28]	69%	Mo	633	13.7	57.3	4.97
[29]	76%	Mo	718	13.1	51	4.8
[10]	1.70 eV	Mo	1003	15.8	67.1	10.7
[12]	1.44 eV	Mo	813	26.9	72.2	15.8
[13]	70%	Mo	643	25.9	73.2	12.2
[14]	1.65 eV	ITO	780	12.8	50.6	5.0
This work	68% and 1.41 eV	FTO	667	23.2	65.5	10.15

insights on the species diffusion dynamics and its interplay with the film's morphology. Such study will be combined with an exhaustive defect analysis using a combination of admittance spectroscopy techniques and Raman spectroscopy.

In addition, this work focused on the improved Ga incorporation when using a Na PreDT, as demonstrated by the XRD/Raman analysis and the bandgap increase; at this point, we do have data to infer other mechanisms through which Na doping would improve the performance of the cells, but such possibility should not be discarded. Also, the mechanism of phase separation in the absence of sodium is currently under investigation by our team, with an interplay with the deposition conditions which will be discussed in a future communication.

Finally, the solar cells reported here do not have an antireflection coating. In wide bandgap CIGSe, such layer would provide a significant current bump, and more than 1% of absolute efficiency gain was previously reported from the addition of an anti-reflection coating (ARC).[10] The tested solar cells do not have a metallic grid, and thus could not be certified. While the measurement's reproducibility is thoroughly assessed during this study (Figure S3, Supporting Information), our future work will focus on improving that specific point for efficiency certification.

3. Conclusion

The work presented here unequivocally demonstrates that wide bandgap CIGSe solar cells can be made with a transparent substrate and retain performances close to the state of the art on metallic nontransparent substrates. With a combination of XRD, GDOES, and Raman analysis, we identify the Na PreDT as a key parameter permitting a better and more homogeneous Ga incorporation to the CIGSe film and markedly reducing the phase segregation, resulting in an overall larger bandgap material with improved PV properties. The electrical characterization of complete solar cell devices shows a spectacular performance improvement with the sodium pretreatment, enhancing both the open-circuit voltage and fill factor of the photodiodes, by way of reducing both the shunts and the recombination parameter J_0, and resulting in a record efficiency over 10% without antireflection coating. Several improvement pathways are given, and this work represents a proof of concept for efficient wide bandgap CIGSe solar cells with a transparent back contact.

4. Experimental Section

Solar Cells Fabrication: The solar cells presented were fabricated with the following material stack: SLG/FTO/Mo/(NaF)/CIGSe/CdS/ZnO/ITO. Also, samples with and without NaF were compared (sample #1 and sample #2).

The SLG/FTO substrate was purchased from Sigma-Aldrich (reference #735183). A thin Mo layer (<15 nm) was deposited by direct current (DC) sputtering on the substrate, to help with the formation of MoSe$_2$ during the reactive annealing stage. The Na PreDT consisted the thermal evaporation of a 15 nm NaF layer for sample #1, whereas sample #2 was the reference without the NaF layer. It was worth noting that FTO was known to efficiently block the diffusion of Na from the SLG substrate, and we made the assumption that the absorber for sample #2 was Na-free.

For the fabrication of the CIGSe absorber, a Cu–In–Ga metal precursor was deposited by DC magnetron sputtering for the Cu and Ga elements, and by thermal evaporator for the In element. A two-step reactive

annealing under Se atmosphere was carried out by placing the metallic precursor samples in a graphite box along with an optimized amount of elemental Se, and the graphite box was inserted in a quartz tubular furnace. In a first step, the temperature was increased from room temperature to 400 °C with a 20 °C min^{-1} increase rate and a constant 1.5 mbar pressure under an Ar flux (pump valve open); the maximum temperature was maintained for 30 min. In a second step, the temperature was increased (same rate) to a maximum value of 550 °C for 15 min, and the pressure was kept at 1 bar (Ar) without an Ar flux (pump valve closed). The samples were let to naturally cool down at the end of the process. Being Cu deficient in general composition, the as-grown films were expected to feature the formation of a Cu(In,Ga)$_3$Se$_5$ OVC phase at the vicinity of the front interface. XRF data were acquired for each 1.25 × 2.5 cm^2 sample on nine different positions, and averaged to obtain what was referred in the text as the sample's composition. This analysis revealed the ratio of $\frac{Cu}{In+Ga} = 0.7 \pm 0.01$ (CGI) and $\frac{Ga}{In+Ga} = 0.68 \pm 0.01$ (GGI) for both samples, which should correspond to a bandgap of $E_g \approx 1.45$ eV.

Before the deposition of the CdS buffer layer by chemical bath deposition (CBD), the as-grown samples were etched for 10 min in a 2% KCN bath. The window layer was completed with a 50 nm i:ZnO layer and a 300 nm ITO layer deposited by DC sputtering. Each sample was mechanically scribed with individual solar cells of dimension 3 × 3 mm^2. However, the record efficiencies were reported here, several sets of samples were fabricated and showed a remarkable consistency. The electrical characterization of the samples was carried out several times to assess any possible light soaking effect, without showing significant variations (less than 0.5% in absolute on the same cell). The fitting of the dark JV curves was made using a 1-diode model code developed in-house. The values reported in this work are based on the total area of the cell. The reported EQE are normalized to 1 and should only be used for relative comparisons, as a strong current discrepancy was observed from the integration of the raw curves (related to calibration issues of the equipment). As samples #1 and #2 had a similar front contact, and as the absorption of the cells was limited by the front contact reflectivity, using normalized curves was deemed appropriate to discuss the bandgap shift between both samples and the absorption onset.

Material Characterization: The as-deposited CIGSe films and complete solar cells were observed by SEM to assess their morphology. The morphological features presented in the following section were based on the SEM analysis of hundreds of micrometers (width) in different cross-sectional preparations to avoid biased results. We chose in this work to present the images of the complete devices in cross section.

The films were analyzed by XRD using a Bruker D8 Advance, with a scanning rate of 0.6° min^{-1}, a step size of 0.010°, and a 2θ range from 10° to 120°, using the Cu Kα radiation ($\lambda = 1.5406$ Å) operating at 40 kV and 40 mA.

GDOES was used to obtain the relative depth composition of the films, analyzing each element profile by a Horiba Jobin Yvon GD Profiler 2 spectrometer, equipped with an anode diameter of 4 mm and 19 element channels.

Raman spectroscopy using a Horiba Jobin-Yvon FHR640 spectrometer was carried out on the bare CIGSe films with a focus on the identification of possible secondary phases and the qualitative evaluation of the crystalline quality. A high energy 325 nm excitation was used to provide surface information (penetration depth <10 nm), and a lower energy 532 nm excitation was used for a more in-depth assessement of the films (penetration depth <60 nm). In both cases, the power density was kept below 25 W cm^{-2} to avoid any substantial heating of the samples. The spectra were acquired on five different positions of a 1.25 × 2.5 cm^2 sample. It is important to note that these systems have not been previously studied under 325 nm excitation, and a direct quantitative spectra comparison between 532 and 325 nm is thus not possible. Our study will then focus on comparing films with and without the Na PreDT under a similar excitation wavelength. To reduce the uncertainty originating from punctual measurements in the Raman spectra, a large spot diameter (of the order of 100 μm) was used, allowing to reduce the impact of the microcrystalline inhomogeneities. This was carried out using a Raman probe specifically developed in our laboratory.

Supporting Information

Acknowledgements

Conflict of Interest

The authors declare no conflict of interest.

Keywords

[1] M. Nakamura, K. Yamaguchi, Y. Kimoto, Y. Yasaki, T. Kato, H. Sugimoto, *IEEE J. Photovoltaics* **2019**, *9*, 1863.

[2] T. Feurer, P. Reinhard, E. Avancini, B. Bissig, J. Löckinger, P. Fuchs, R. Carron, T. P. Weiss, J. Perrenoud, S. Stutterheim, S. Buecheler, A. N. Tiwari, *Prog. Photovoltaics: Res. Appl.* **2017**, *25*, 645.

[3] A. K. Shukla, K. Sudhakar, P. Baredar, *Energy Buildings* **2017**, *140*, 188.

[4] I. Mathews, S. N. Kantareddy, T. Buonassisi, I. M. Peters, *Joule* **2019**, *3*, 1415.

[5] T. Nakada, Y. Hirabayashi, T. Tokado, D. Ohmori, T. Mise, *Sol. Energy* **2004**, *77*, 739.

[6] N. Cavallari, F. Pattini, S. Rampino, F. Annoni, M. Barozzi, M. Bronzoni, E. Gilioli, E. Gombia, C. Maragliano, M. Mazzer, G. Pepponi, G. Spaggiari, R. Fornari, *Appl. Surface Sci.* **2017**, *412*, 52.

[7] Z. Yu, *Nat. Energy* **2016**, *1*, 1.

[8] G. Hanna, A. Jasenek, U. Rau, H. W. Schock, *Thin Solid Films* **2001**, *387*, 71.

[9] Q. Cao, O. Gunawan, M. Copel, K. B. Reuter, S. J. Chey, V. R. Deline, D. B. Mitzi, *Adv. Energy Mater.* **2011**, *1*, 845.

[10] F. Larsson, N. S. Nilsson, J. Keller, C. Frisk, V. Kosyak, M. Edoff, T. Törndahl, *Prog. Photovoltaics: Res. Appl.* **2017**, *25*, 755.

[11] T. Eisenbarth, T. Unold, R. Caballero, C. A. Kaufmann, D. Abou-Ras, H.-W. Schock, *Thin Solid Films* **2009**, *517*, 2244.

[12] M. A. Contreras, L. M. Mansfield, B. Egaas, J. Li, M. Romero, R. Noufi, E. Rudiger-Voigt, W. Mannstadt, *Prog. Photovoltaics: Res. Appl.* **2012**, *20*, 843.

[13] C. P. Muzzillo, L. M. Mansfield, C. Dehart, K. Bowers, R. C. Reedy, B. To, R. Noufi, K. Ramanathan, T. J. Anderson, in *IEEE 40th Photovoltaic Specialist Conf.*, IEEE, Denver, CO, pp. 649–1654.

[14] J. H. Choi, K. Kim, Y.-J. Eo, J. H. Park, J. Gwak, S.-K. Ahn, A. Cho, S. Ahn, J.-S. Cho, K. Shin, K. Yoon, S. H. Kong, J.-H. Yun, J. Yoo, *Vacuum* **2015**, *120*, 42.

[15] A. Chirilă, P. Reinhard, F. Pianezzi, P. Bloesch, A. R. Uhl, C. Fella, L. Kranz, D. Keller, C. Gretener, H. Hagendorfer, D. Jaeger, R. Erni, S. Nishiwaki, S. Buecheler, A. N. Tiwari, *Nat. Mater.* **2013**, *12*, 1107.

[16] M. Gloeckler, J. R. Sites, *J. Phys. Chem. Solids* **2005**, *66*, 1891.

[17] C. A. Kaufmann, R. Caballero, T. Unold, R. Hesse, R. Klenk, S. Schorr, M. Nichterwitz, H.-W. Schock, *Sol. Energy Mater. Sol. Cells* **2009**, *93*, 859.

[18] H. Miyazaki, R. Mikami, A. Yamada, M. Konagai, *J. Phys. Chem. Solids* **2003**, *64*, 2055.

[19] W. Witte, R. Kniese, A. Eicke, M. Powalla, *IEEE 4th World Conf. on Photovoltaic Energy Conf.*, Vol. 1, IEEE, Waikoloa, HI **2006**, pp. 553–556.

[20] J. Müller, J. Nowoczin, H. Schmitt, *Thin Solid Films* **2006**, *496*, 364.

[21] A. Moreau, C. Insignares-Cuello, L. Escoubas, J.-J. Simon, V. Bermúdez, A. Pérez-Rodríguez, V. Izquierdo-Roca, C. M. Ruiz, *Sol. Energy Mater. Sol. Cells* **2015**, *139*, 101.

[22] M. Wang, M. A. Hossain, K.-L. Choy, *Sci. Rep.* **2017**, *7*, 1.

[23] W. Witte, R. Kniese, M. Powalla, *Thin Solid Films* **2008**, *517*, 867.

[24] C. Rincón, F. J. Ramirez, *J. Appl. Phys.* **1992**, *72*, 4321.

[25] D. Fraga, T. Stoyanova Lyubenova, R. Martí, I. Calvet, E. Barrachina, J. B. Carda, *Sol. Energy* **2017**, *147*, 1.

[26] C. Insignares-Cuello, C. Broussillou, V. Bermúdez, E. Saucedo, A. Pérez-Rodríguez, V. Izquierdo-Roca, *Appl. Phys. Lett.* **2014**, *105*, 021905.

[27] M. Raghuwanshi, E. Cadel, P. Pareige, S. Duguay, F. Couzinie-Devy, L. Arzel, N. Barreau, *Appl. Phys. Lett.* **2014**, *105*, 013902.

[28] T. Higuchi, N. Usami, T. Minemoto, *Phys. Status Solidi C* **2013**, *10*, 1035.

[29] R. Baier, J. Lehmann, S. Lehmann, T. Rissom, C. Alexander Kaufmann, A. Schwarzmann, Y. Rosenwaks, M. Lux-Steiner, *Sol. Energy Mater. Sol. Cells* **2012**, *103*, 86.

[30] A. Cuevas, *Energy Proc.* **2014**, *55*, 53.